SatERR: A Community Error Inventory for Satellite Microwave Observation Error Representation and Uncertainty Quantification

John Xun Yang,[a,b] Yalei You,[c] William Blackwell,[d] Cheng Da,[a] Eugenia Kalnay,[e] Christopher Grassotti,[a,b] Quanhua (Mark) Liu,[b] Ralph Ferraro,[a] Huan Meng,[b] Cheng-Zhi Zou,[b] Shu-Peng Ho,[b] Jifu Yin,[a,b] Veljko Petkovic,[a,b] Timothy Hewison,[f] Derek Posselt,[g] Antonia Gambacorta,[h] David Draper,[i] Sidharth Misra,[g] Rachael Kroodsma,[h] and Min Chen [j]

[a] *Earth System Science Interdisciplinary Center/ Cooperative Institute for Satellite Earth System Studies, University of Maryland, College Park, MD USA*

[b] *NOAA Center for Satellite Applications and Research, National Environmental Satellite, Data, and Information Service, College Park, MD, USA*

[c] *Department of Earth and Ocean Sciences, University of North Carolina, Wilmington, NC USA*

[d] *MIT Lincoln Laboratory, Lexington, MA USA*

[e] *Department of Atmospheric and Oceanic Science, University of Maryland, College Park, MD USA*

[f] *European Organisation for the Exploitation of Meteorological Satellites (EUMETSAT), Darmstadt, Germany*

[g] *NASA Jet Propulsion Laboratory, Pasadena, CA USA*

[h] *NASA Goddard Space Flight Center, Greenbelt, MD USA*

[i] *Ball Aerospace and Technology Corporation, Boulder, CO USA*

[j] *University of Wisconsin, Madison, WI USA*

Corresponding author: John Xun Yang, jxyang@umd.edu

Early Online Release: This preliminary version has been accepted for publication in *Bulletin of the American Meteorological Society*, may be fully cited, and has been assigned DOI 10.1175/BAMS-D-22-0207.1. The final typeset copyedited article will replace the EOR at the above DOI when it is published.

ABSTRACT: Satellite observations are indispensable for weather forecasting, climate change monitoring, and environmental studies. Understanding and quantifying errors and uncertainties associated with satellite observations are essential for hardware calibration, data assimilation, and developing environmental and climate data records. Satellite observation errors can be classified into four categories: measurement, observation operator, representativeness, and preprocessing errors. Current methods for diagnosing observation errors still yield large uncertainties due to these complex errors. When simulating satellite errors, empirical errors are usually used, which do not always accurately represent the truth. We address these challenges by developing an error inventory simulator, the **Sat**ellite **E**rror **R**epresentation and **R**ealization (SatERR). SatERR can simulate a wide range of observation errors, from instrument measurement errors to model assimilation errors. Most of these errors are based on physical models, including existing and newly-developed algorithms. SatERR takes a bottom-up approach: Errors are generated from root sources and forward propagate through radiance and science products. This is different from, but complementary to, the top-down approach of current diagnostics, which inversely solves unknown errors. The impact of different errors can be quantified and partitioned, and a ground-truth testbed can be produced to test and refine diagnostic methods. SatERR is a community error inventory, open-source on GitHub, which can be expanded and refined with input from engineers, scientists, and modelers. This debut version of SatERR is centered on microwave sensors, covering traditional large satellites and small satellites operated by NOAA, NASA, and EUMETSAT.

Accepted for publication in *Bulletin of the American Meteorological Society.* DOI 10.1175/BAMS-D-22-0207.1.

CAPSULE: A bottom-up error inventory simulator has been developed at NOAA to quantify and partition a wide range of satellite observation errors.

1. Introduction

Satellites have played an indispensable role in Earth system studies. For numerical weather prediction (NWP), satellite data assimilated into numerical models are a dominant contributor to the overall reduction of forecast errors and uncertainties (Kalnay 2003; Langland and Baker 2004; Joo et al. 2013; Geer et al. 2018). Compared to ground-based observations, satellites have advantage of global coverage. In particular, microwave radiometers can perform measurements under clear and cloudy conditions. In climate studies, satellite radiometers have shown the capability to detect subtle climatological signals such as atmospheric temperature trend with a magnitude of a couple of tenths of Kelvins per decade (Spencer and Christy 1992a,b; Christy et al. 1997; Vinnikov and Grody 2003; Zou and Wang 2011; Mears and Wentz 2017; Zou et al. 2021). Measurement accuracy and precision cannot be accomplished without understanding the range of error and uncertainty sources associated with observations. An error is the difference between a measured value and the truth, which can be random (e.g., noise) or systematic (e.g., imperfect calibration) (Kalnay 2003; Merchant et al. 2017; Bormann 2020). Uncertainty indicates the dispersion of a measured quantity. Quantifying observation errors is highly important and of continuous interest to the science community.

In the context of data assimilation (DA), observation errors can be classified into four categories: measurement, observation operator, representativeness, and preprocessing (quality control) (Kalnay et al. 1996; Geer and Bauer 2011; Bormann and Bauer 2010; Zou and Wang 2011; Janjić et al. 2018; Carrassi et al. 2018). Measurement errors stem from instruments as bias and noise in the measured radiance. Observation operator errors are due to deficiencies in the forward model, such as a radiative transfer model (RTM) when assimilating satellite observations. Representativeness errors account for unresolved scales and processes, related to model parameterization and scale resolution. The preprocessing error relates to the data prescreening process, such as rejecting observations that cannot be adequately modeled or retrieving state variables that can be better modeled. The measurement error is instrument related, and the other three can be referred to as representation errors. In practice, errors arise from multiple underlying sources of the four cate-

Accepted for publication in *Bulletin of the American Meteorological Society.* DOI 10.1175/BAMS-D-22-0207.1.

gories. They are rarely modeled properly as individual error sources and are often mixed together, resulting in incorrect characterization and evaluation of the uncertainty. Data assimilation requires quantifying the observation error in terms of its error covariance to determine how different observations are weighted within the analysis system. Data assimilation distinguishes between random and systematic errors relating to observations. A statistical description of the random errors is used to assign weights to the observations, and this is also referred to as observation error. Systematic errors are removed through bias correction, based on an adequate model for the bias. We refer to observation error as both random and systematic errors in this article.

In addition to data assimilation, assessing satellite observation errors and uncertainties is also essential for the development and application of Environmental Data Records (EDRs) and Climate Data Records (CDRs) from satellite observations (National Research Council 2007; Zou and Wang 2011; Hollmann et al. 2013; Ablain et al. 2015; Merchant et al. 2017; Bellprat et al. 2017; Merchant et al. 2019; Gruber et al. 2020; Mittaz et al. 2019). For instance, satellite orbit drift or sensor electronics degradation can change long-term radiances and retrieved geophysical variables, as seen in microwave sounders operated by the National Oceanic and Atmospheric Administration (NOAA) and the European Organisation for the Exploitation of Meteorological Satellites (EUMETSAT) (Hurrell and Trenberth 1997; Zou and Wang 2011; Lu and Bell 2014; Zou et al. 2018; Yang et al. 2021). Anomalies and jumps are also observed in CDRs and reanalyses due to inappropriate treatment of biases and model issues (Newman et al. 2000; Dee et al. 2014; Santer et al. 2017). An accurate error estimate allows for the correction or reduction of the biases in these EDR and CDR products, as shown by research at the European Centre for Medium-Range Weather Forecasts (ECMWF) and NOAA (Saha et al. 2010; Zou and Qian 2016; Merchant et al. 2017; Mittaz et al. 2019).

Although the measurement error is a subset of the observation error, it is at the core of satellite-observed radiance data, propagating from the instrument level through data assimilation and science products. There are a range of measurement error sources that can affect radiances, such as reflector emission (Wentz et al. 2001; Gopalan et al. 2009; Geer et al. 2010; Kim et al. 2014), polarization angle misalignment (Weng et al. 2003; Yang et al. 2012), field-of-view (FOV) intrusion (Twarog et al. 2006; McKague et al. 2010), and warm load error caused by solar intrusion (Twarog et al. 2006; McKague et al. 2010), among others. Errors can also stem from receivers, including cross-

Accepted for publication in *Bulletin of the American Meteorological Society.* DOI 10.1175/BAMS-D-22-0207.1.

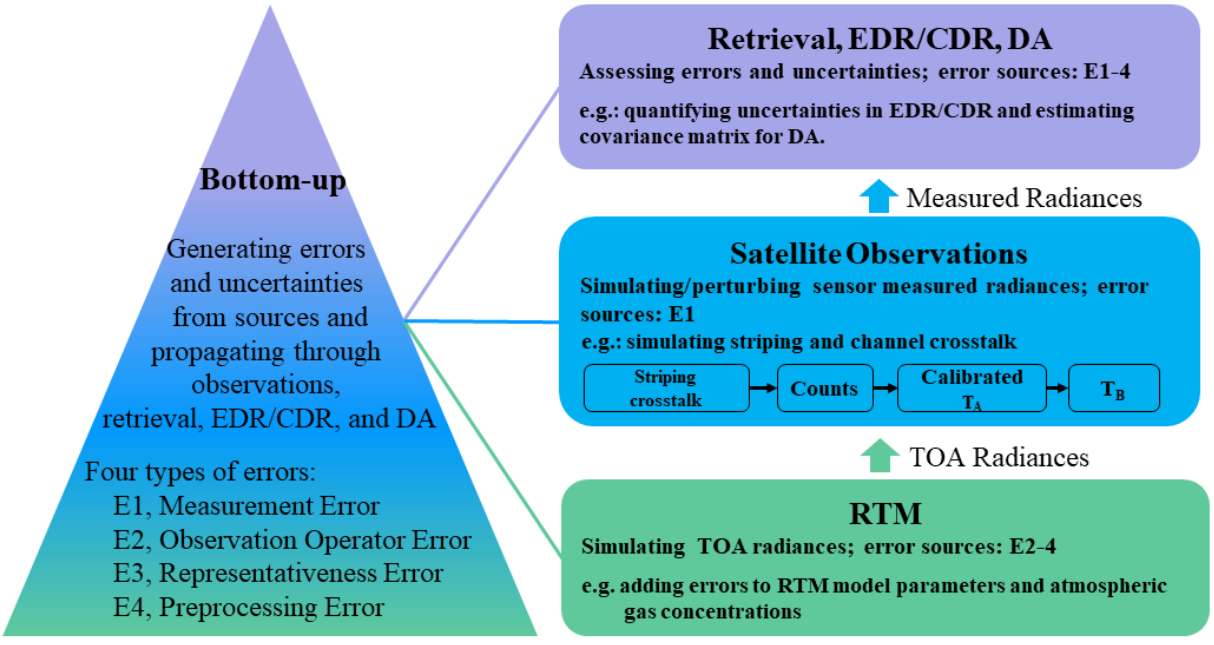

FIG. 1. SatERR is a bottom-up approach, where the four types of errors including measurement, preprocessing, observation operator, and representativeness errors are generated from sources and forward propagate through radiances, science products, and data assimilation systems. This approach can quantify and partition errors and uncertainties in science products, and capture leading features of the most important errors in a statistical sense for data assimilation.

polarization leakage (Balanis 2015), impedance mismatch (Ruf et al. 1995; Piepmeier et al. 2017), and long-term calibration drift (Wentz and Schabel 1998; Zou and Wang 2011; Lu and Bell 2014). Electronic noise is intrinsic in satellite sensors and is a critical uncertainty source that degrades radiometer sensitivity and science products (Weng et al. 2013; Qin et al. 2013; Bormann et al. 2013; Yang et al. 2021). Error contributors have also been found in onboard instrument interference (Draper et al. 2015), spacecraft attitude offsets (Meissner and Wentz 2006; Kroodsma et al. 2012), and radio frequency inference (Njoku et al. 2005; Piepmeier et al. 2013). The processing of satellite radiance data from raw counts to brightness temperatures to intercalibration across sensors can introduce errors (Njoku 1980; Janssen et al. 1995; Yang et al. 2015b; Berg et al. 2016). Once in orbit, satellite measurement errors cannot be as easily examined as on the ground. The treatment of errors in the assimilation process is often simplified, which is the consequence of several factors, such as technical limitations, magnitudes of error sources and our ability to quantify them, and

Accepted for publication in *Bulletin of the American Meteorological Society.* DOI 10.1175/BAMS-D-22-0207.1.

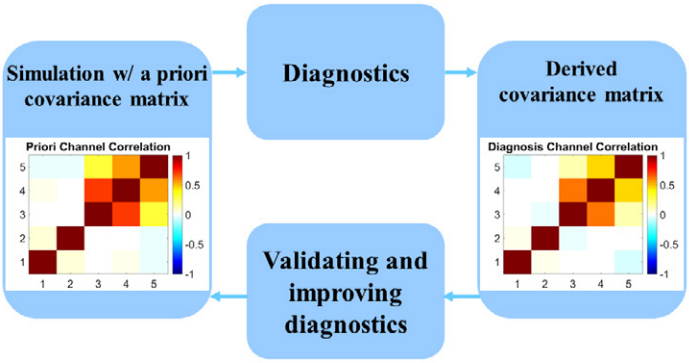

FIG. 2. A schematic showing the generation of a testbed with SatERR for validating and improving diagnostics in terms of the covariance of interchannel correlation.

maintainability of uncertainty modeling that may change over time (Bell et al. 2008; Janjić et al. 2018).

While notable efforts have been made toward quantifying observation errors, critical challenges have yet to be addressed. Simulating an error at the pixel level using physical models can provide superior uncertainty information compared to using simple statistical errors (Merchant et al. 2017; Mittaz et al. 2019). Furthermore, it is challenging to partition different error sources due to their complexity and coupling. A diagnostic specialized on one error cannot exclude the impact of other errors. For instance, an interchannel correlation can stem from hardware crosstalk (Corbella et al. 2002; Kim et al. 2014), the observation operator, and geophysical parameters (Campbell et al. 2017; Stewart et al. 2014; Bormann 2020). An effective means of validation is desired for these diagnostics. Apart from technical challenges, there are apparent barriers within the science community. Error corrections applied on low-level radiance data are insufficiently communicated to scientists working on data assimilation and EDR/CDR, and vice versa. Due to the somewhat compartmentalized nature of satellite data generation and processing, the chain of uncertainty quantification is typically broken.

The primary objective of this work is to address the aforementioned challenges through the development of a comprehensive error inventory simulator. This simulator is named the **Sat**ellite **E**rror **R**epresentation and **R**ealization (SatERR). SatERR is developed to generate various observation errors to differentiate the impact of different errors, assess error propagation, and test diagnostic methods. It takes a bottom-up approach: Errors are generated from root sources and forward

Accepted for publication in *Bulletin of the American Meteorological Society*. DOI 10.1175/BAMS-D-22-0207.1.

propagate through radiance and science products. This is different from, but complementary to, the top-down approach of current diagnostics, which inversely solves for unknown errors (Bormann 2020). Fig. 1 illustrates the conceptual outline of SatERR. The simulated Top of Atmosphere (TOA) radiances translate to sensor-measured radiances through measurement processes down to count level, and feeds applications in EDR/CDR and data assimilation. SatERR could inform the assignment of observation errors for random errors or the modeling of systematic errors as needed for bias correction. Fig. 2 shows an example, where a ground-truth testbed with known interchannel correlation can be generated for testing and validating diagnostics. SatERR is designed to use separate modules that can be called individually and combined with existing models, leaving room for easy expansion and addition of new error sources into the inventory. The open-source script and bottom-up structure bridge the gap of separated errors and bring together scientists working on different stages. The current version of SatERR is centered on microwave radiometers, while many of the modules can be used for visible and infrared (VIR) sensors and future expansion will cover more VIR instruments and applications. The rest of the paper is organized as follows. In section II, we lay out the simulator structure and individual modules. Section III shows examples and validations, followed by a summary in section IV. Additional technical details can be found in the SatERR User Manual on GitHub.

2. Error Inventory Overview

SatERR estimates the effects of errors and error propagation by calculating brightness temperature (or geophysical parameters derived from brightness temperature) differences between two simulations, in which one simulation with one or multiple parameters perturbed by a specified magnitude is compared to the other simulation that is perturbation free. This approach allows for taking the non-linear effects of error propagation into account, in contrast to some other approaches such as the tangent linear model.

SatERR is open source on GitHub (`https://github.com/jxyangrs/saterr`). This paper provides a brief overview and examples due to the limited space, while technical details, model physics and usage can be found in the User Manual (`https://github.com/jxyangrs/saterr/blob/main/manual_saterr.pdf`). The basic modules and functions are introduced in the following sections. Fig. 3 illustrates the main modules of SatERR with the corresponding

Accepted for publication in *Bulletin of the American Meteorological Society.* DOI 10.1175/BAMS-D-22-0207.1.

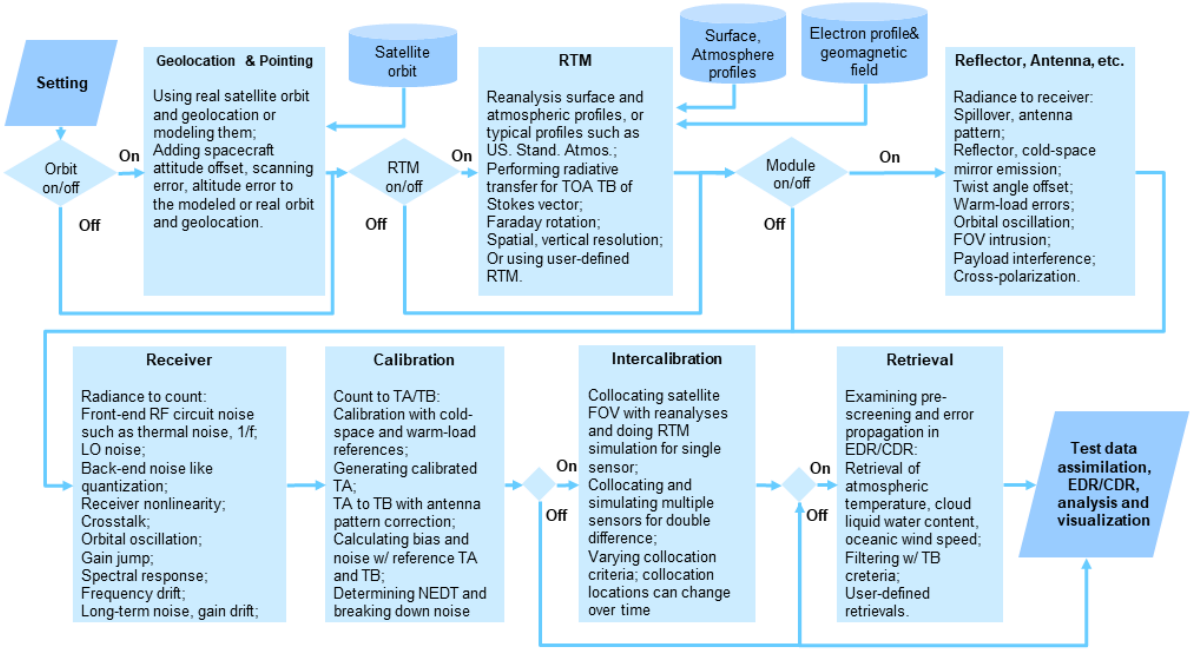

FIG. 3. SatERR simulates a wide range of individual and compound errors contained in corresponding modules. It covers a chain of satellite observations, including orbit and geolocation, RTM, sensor measurement (counts to calibrated radiances), intercalibration, and retrievals, which can feed applications in science products and data assimilation.

error sources described. The simulation flow and error propagation cover a chain of satellite observations, including orbit and geolocation, RTM for simulating TOA radiances which are then processed to counts and calibrated radiances, intercalibration, and retrievals. The final output can include calibrated radiances and several geophysical variables from the provided retrieval algorithms, which can be further fed to data assimilation systems and sophisticated retrieval algorithms. Intermediate parameters such as satellite geolocation and counts can also be exported for specific applications.

SatERR is centered on spaceborne microwave sensors, but many modules can also be applied to visible and infrared sensors. Table 1 lists satellite sensors that can be simulated by SatERR, covering 15 instruments onboard both large satellite missions and small satellites. SatERR can also be used to develop and analyze new sensors and systems with customized specifications. A list of error sources is summarized in Table A1 in the Appendix. The simulator is a collection of MATLAB and Python codes. It needs no compiling or sophisticated installation. The simulator is

Accepted for publication in *Bulletin of the American Meteorological Society*. DOI 10.1175/BAMS-D-22-0207.1.

TABLE 1. The SatERR Sensor Family.

Imager	Sounder
Advanced Microwave Scanning Radiometer for EOS (AMSR-E)	Advanced Microwave Sounding Unit - A (AMSU-A)
Advanced Microwave Scanning Radiometer - 2 (AMSR2)	Advanced Microwave Sounding Unit - B (AMSU-B)
GPM Microwave Imager (GMI)	Advanced Technology Microwave Sounder (ATMS)
Microwave Radiation Imager (MWRI)	MicroWave Temperature Sounder II (MWTS-2)
	MicroWave Humidity Sounder II (MWHS-2)
Soil Moisture Active-Passive (SMAP)	MicroWave Humidity Sounding (MHS)
Special Sensor Microwave/Imager (SSM/I)	Temporal Experiment for Storms and Tropical Systems – Demonstration (TEMPEST-D)
Special Sensor Microwave - Imager/Sounder (SSMIS)	Time-Resolved Observations of Precipitation structure and storm Intensity with a Constellation of Smallsats (TROPICS)
Customization/New Sensors	Customization/New Sensors

highly vectorized for fast computing, such as running the RTM, orbit simulations, and collocation. It is designed for application in a Linux-like environment, allowing for the breakdown of tasks and submission of multiple jobs to hundreds or thousands of cores. The code can also run in a PC or Mac for simple simulations. The simulator package is mostly comprised of scripts and several demonstration datasets, with a total size of 3 MB. The source code contains more than 30,000 lines of code with over 300 scripts.

Geolocation and Pointing

The geolocation and pointing module generates errors associated with the spacecraft orbit, sensor scanning geometry, and FOV geolocation. Observations can be fed into the simulator. Spacecraft attitude errors such as pitch, roll, and yaw can be set, and sensor-scanning errors can be counted for both cross-track and conical-scanning radiometers. Given the orbit and sensor-scanning geometry and added errors, new FOV geolocation and local angles are determined with a module for transforming between local and Earth coordinate systems (Cai et al. 2011). Additionally, a module based on the Keplerian orbit model is included for modeling the orbits of polar-orbiting and low-inclination satellites, providing six orbit elements (Griffin 2004).

RTM

The RTM module includes a 1-D RTM for microwave to study observation-operator errors (Rosenkranz 2017; Rosenkranz and Cimini 2019). An ocean emissivity model is included (El-

Accepted for publication in *Bulletin of the American Meteorological Society.* DOI 10.1175/BAMS-D-22-0207.1.

saesser 2006). The ionosphere module calculates the Faraday rotation, which occurs when an electromagnetic wave goes through the ionosphere. A module comprising the International Geomagnetic Reference Field model computes the geomagnetic field (Thébault et al. 2015). Submodules for downloading, processing, and collocating reanalysis data like ERA-5 and NCEP are also included. The authors are aware of many established RTMs, such as the Radiative Transfer for TOVS (RTTOV) and the Community Radiative Transfer Model (CRTM), covering visible, infrared and microwave spectra (Han 2006; Saunders et al. 2018). Users can run these RTMs and feed the simulation results to SatERR. Errors can be added to the Rosenkranz microwave absorption spectrum by tuning parameters such as line intensity and width. Parameters such as the number of vertical discrete levels and horizontal resolution can be adjusted, since they show an impact on the simulated radiances. State variables of atmosphere and surface can be perturbed to examine their impact on simulations.

Both RTTOVS and CRTM now have all-sky components. For example, the NOAA Global Forecast System (GFS), with CRTM as its observation operator, has recently been updated with many skills for all-sky assimilation (Liu et al. 2022), where there are a number of components SatERR can support by providing useful error information. These updates include the replacement of the Temperature Data Record (TDR) with Sensor Data Record (SDR) for ATMS, assimilation under thick cloudy conditions over the ocean, and precipitation filtering (Liu et al. 2022). For example, SatERR can verify the new bias correction when replacing TDR with SDR, and the impact of fractional cloud coverage on the radiances can be estimated with SatERR simulation.

We recognize that the RTM error sources in the current version are relatively simple, while RTM errors are essential, and a range of aspects can be perturbed, including gas absorption spectra, aerosol/cloud/rain, and oceanic and land surface models. We will expand the RTM errors in the next version and maximize the use of external RTMs for RTM error representation.

Antenna and Receiver

The antenna sub-system and receiver modules include errors associated with antenna pattern (mainlobe, sidelobe, and spillover) (Njoku 1980; Janssen et al. 1995), cross-polarization contamination (Balanis 2015), the twist angle offset (Weng et al. 2003; Yang et al. 2012), FOV intrusion (Colton and Poe 1999; McKague et al. 2010), reflector emission (Weng 2015), and instrumental

Accepted for publication in *Bulletin of the American Meteorological Society.* DOI 10.1175/BAMS-D-22-0207.1.

interference (Draper et al. 2015; Wentz and Draper 2016). The antenna pattern affects measured radiances, and parameters such as fraction of mainlobe, sidelobe and backlobe can be adjusted. Modeling antenna pattern is provided with both Bessel and Gaussian shaped patterns (Yang et al. 2014). The antenna patterns can be projected on the ground with Geolocation and Pointing module to study FOV covolution. A set of noise models are developed to simulate receiver electronic noise and other error sources such as thermal noise, shot noise, and flicker noise from the radio frequency integrated circuit (RFIC) (Lee 2004; Yang et al. 2021, 2022). Modules are also provided for the receiver nonlinearity, gain fluctuation, and receiver orbit oscillation (Gaiser et al. 2004).

Calibration and Intercalibration

The calibration module enables studying errors associated with processing counts into antenna temperature (TA) and brightness temperature (TB). The processing of receiver counts to TA and TB can give rise to errors due to antenna pattern correction and calibration techniques (Njoku 1980; Yang et al. 2022). The intercalibration module evaluates uncertainties associated with satellite constellation cross-calibration, which is affected by a range of factors, including collocation criteria (distance and time interval), scanning angles, cloud screening, and ancillary profiles in the RTM simulation (Chander et al. 2013; Yang et al. 2015a; Yang and McKague 2016). The observation minus background (O-B) of RTM simulations, also referred to as single difference, and the inter-sensor difference (double difference) can be derived, and their impact quantified (Berg et al. 2016).

Retrieval

The retrieval module evaluates the impact of radiance errors on science products. For instance, empirical algorithms are included for retrieving atmospheric temperature, cloud liquid water content, and oceanic surface wind speed (Goodberlet et al. 1989; Rosenkranz 2006; Zhu and Weng 2013). This module can also be used in intercalibration for screening clouds and precipitation. Users can refer to other established algorithms for producing EDR and CDR products, such as a 1DVar retrieval algorithm, the Microwave Integrated Retrieval System (MiRS), at NOAA (Boukabara et al. 2011; Liu et al. 2020; Lee et al. 2022). Lastly, we provide a number of scripts for visualizing and analyzing the output, e.g., time and frequency domain analyses.

Accepted for publication in *Bulletin of the American Meteorological Society.* DOI 10.1175/BAMS-D-22-0207.1.

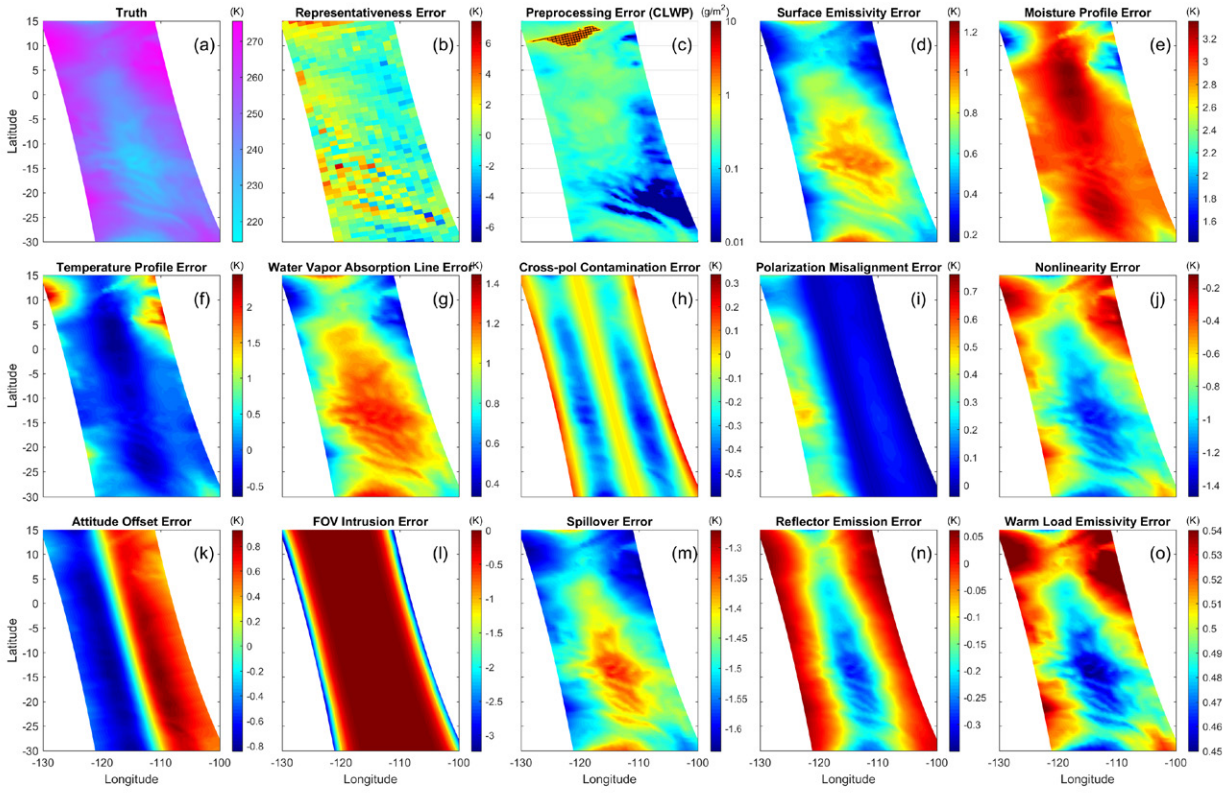

FIG. 4. Examples of simulated observation errors for AMSU-A at 89 GHz on 1 January 2021: (a) Simulated error-free brightness temperature. (b) Representativeness error due to a coarse horizontal resolution. (c) Preprocessing error due to retrievals (screening pixels with high cloud liquid water paths). (d) Ocean emissivity model error. (e) Moisture profile error. (f) Temperature profile error. (g) Water vapor absorption line error. (h) Cross-polarization contamination error. (i) Polarization misalignment. (j) Radiometer nonlinearity. (k) Spacecraft attitude offset. (l) FOV intrusion. (m) Spillover error from the cosmic background. (n) Reflector emission. (o) Warm load emissivity error. These observation errors are situation dependent with varying patterns and magnitudes.

3. Results

Observation Error Examples

Fig. 4 illustrates a number of observation errors simulated by SatERR. The simulation is for MetOp-A AMSU-A on 1 January 2021, showing a swath for channel 15 (89 GHz) and quasi-vertical polarization. ERA5 reanalyses with 137 vertical layers and a 0.25 degree horizontal resolution are

Accepted for publication in *Bulletin of the American Meteorological Society*. DOI 10.1175/BAMS-D-22-0207.1.

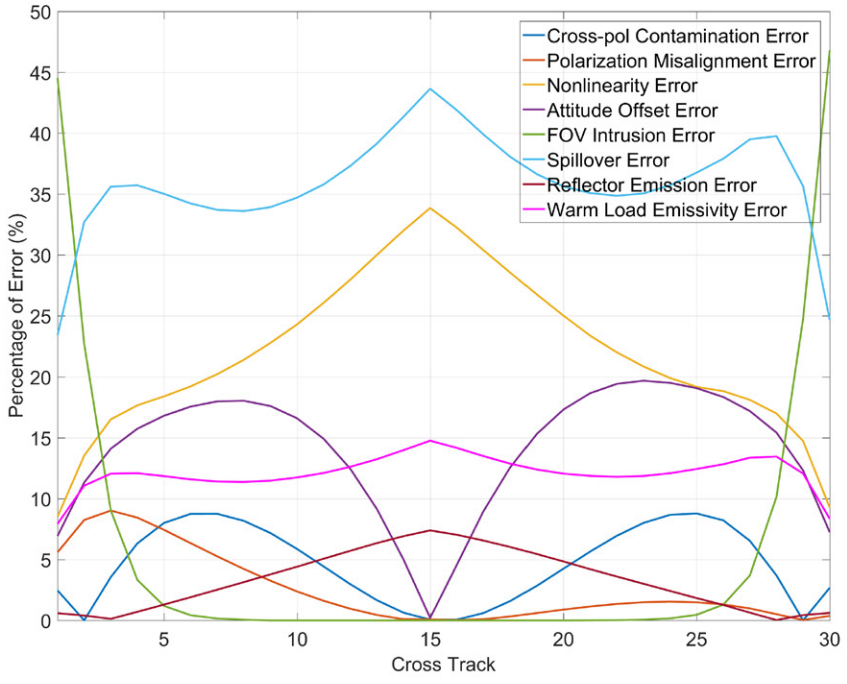

FIG. 5. SatERR-quantified percentage of different measurement errors as a function of cross-track scan.

used as input to the RTM. We first simulate the error-free brightness temperature (Fig. 4a), then turn on different error sources in the simulation. Subtracting errors from the error-free brightness temperature allows us to examine error features. Fig. 4b shows the representativeness error when performing the RTM simulation with a coarse horizontal spatial resolution. The satellite FOV is gridded to 0.3×0.2 degrees horizontally, reducing the FOV numbers by half in both cross-track and along-track directions, and simulation is performed twice before and after the gridding to show the difference between the grid and the closest FOV. The retrieved cloud liquid water path (CLWP) from AMSU-A radiance is shown in Fig. 4c, with high-CLWP pixels marked. Preprocessing errors can arise from screening high CLWP when there are deficiencies in the retrieval algorithm. In Fig. 4d, the error is from increasing the oceanic emissivity by 1% (Elsaesser 2006). Fig. 4e and f are errors by perturbing the atmospheric moisture and temperature profiles by 5% and 2% increase, respectively. Fig. 4g is from tuning the parameter of water vapor absorption intensity by a 5% increase in the Rosenkranz model (Rosenkranz 2017).

Other observation errors include cross-polarization contamination (Fig. 4h) due to radiance contamination between channels with opposite polarizations. Here, 5% cross-polarization con-

Accepted for publication in *Bulletin of the American Meteorological Society.* DOI 10.1175/BAMS-D-22-0207.1.

tamination is assumed (Weng et al. 2013). A polarization misalignment (Fig. 4i) can arise from reflector angular offset in the mechanical alignment (Weng et al. 2003; Yang et al. 2012). A 0.2° offset is used for the three alignment angles. An error due to receiver nonlinearity (e.g., 2 K) is also illustrated in Fig. 4j (Mo 1996). The spacecraft attitude can have offsets in roll, pitch, and yaw (Meissner and Wentz 2006; Kroodsma et al. 2012). A 0.2 degree perturbation of the three angles is used in this demonstration (Fig. 4k). Spacecraft can intrude into the radiometer FOV, especially at the edge of the scan, as shown in Fig. 4l using AMSU-A empirical intrusion parameters (Colton and Poe 1999; McKague et al. 2010). All radiometers have spillover because the antenna pattern sees out of the reflector. A 0.3% spillover is assumed in Fig. 4m (Yan and Ahmad 2020). The reflector can be an emission source with an emissivity larger than zero (Wentz et al. 2001; Gopalan et al. 2009; Kim et al. 2014). In Fig. 4n, emissivities of 0.01 and 0.05 are used for the V and H polarizations, respectively. The onboard warm load is supposed to be a perfect blackbody, but its emissivity can be less than one in practice, as shown in Fig. 4o with 0.998% emissivity (Twarog et al. 2006; Alquaied et al. 2018).

These observation errors are situation dependent, i.e., errors are not fixed but vary with Earth-scene dynamics. These errors are not simply additive but a combination of multiplicative and additive terms with a partial dependence on the Earth scene itself. None of these errors are identical in terms of patterns and magnitudes, and some errors show similar patterns. This implies there is scope for compensating errors, posing difficulty to attribute errors seen for real observations to error sources. Results indicate that a fixed error cannot represent the truth. The situation becomes complicated when different errors are mixed. The magnitudes of observation errors of the four categories are dependent on channels (Chun et al. 2015; Bormann 2020). For example, microwave upper-atmosphere sounding channels usually have relatively large measurement error (instrument noise) and small observation-operator error, while lower-atmosphere sounding and window channels are the opposite. We will conduct an extensive simulation to quantify and order the magnitudes of the four categories.

In the following two sections, we present two examples to demonstrate how SatERR can be used to study error quantification and propagation.

Accepted for publication in *Bulletin of the American Meteorological Society.* DOI 10.1175/BAMS-D-22-0207.1.

Radiometer Striping

Radiometer striping features sharp and non-periodic stripes with large fluctuations, found in radiance data (Jarnot et al. 1996; Qin et al. 2013; Kim et al. 2014; Yang et al. 2021), and affecting science products (Ma and Zou 2015) and data assimilation (Bormann et al. 2013; Popp et al. 2020). Striping appears directional in the cross-track direction. It is related to the 1/f noise in semiconductor electronics (Lee 2004; Davis and Agarwal 2011). Recent studies have also shown that it can arise from thermal and 1/f noise with different features (Yang et al. 2021, 2022).

Striping is non-stationary, with statistical properties of mean and variance changing over time, which is in contrast with stationary noise such as the typical Gaussian additive white noise (Lee 2004; Kim et al. 2014; Yang et al. 2021, 2022). The noise of an electronic device such as a radiometer is generally a combination of both stationary and nonstationary noise. In space mission design, noise is simulated and added into radiance to evaluate the radiometer performance and the impact on downstream science applications so that it meets the mission requirement. In data assimilation, noise simulation along with other errors are also conducted to estimate the variance of observation error. Currently, stationary noise is almost exclusively used in simulations, which overlooks non-stationary noise. A method for accurate striping noise simulation, quantification, and decomposition is needed.

SatERR is the first published simulator with a module for striping simulation, quantification, and decomposition (Yang et al. 2021, 2022). For the striping simulation, we consider the presence of radiometer noise (1/f and thermal noise) and orbital oscillation (the oscillation of sensor statuses such as temperature and gain). Both 1/f and thermal noise produce cross-track stripes. The 1/f noise generates sharp stripes, while the thermal noise has smoother, banded features. The simulation adds noise into the counts, which are then processed through calibration to radiances. For noise quantification and decomposition, our algorithms determine the magnitude of in-orbit striping from cold-space and warm-load scenes that are not affected by Earth-scene dynamics. We provide a time-domain algorithm to separate noise into thermal and 1/f noise. A set of tools including the principal component analysis (PCA) and Allan variance spectra are provided to characterize and compare different noise. The simulations have been validated against observations, showing consistent striping characteristics (Yang et al. 2021, 2022).

Accepted for publication in *Bulletin of the American Meteorological Society.* DOI 10.1175/BAMS-D-22-0207.1.

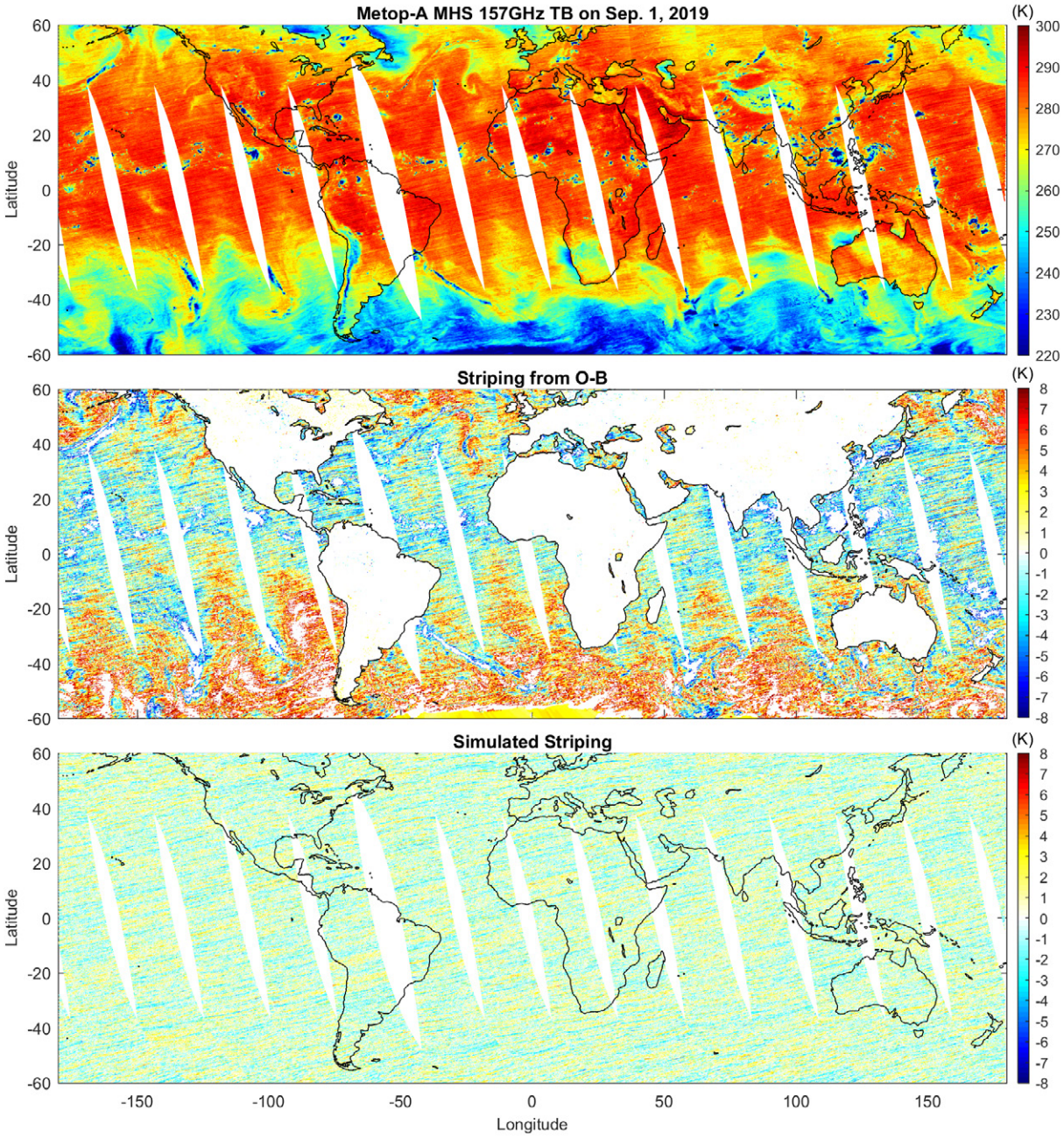

FIG. 6. Striping from observations and simulations. (Top) Metop-A MHS brightness temperature at 157 GHz (unit: K) on 1 September 2019 with noticeable cross-track striping. (Middle) O-B showing clear cross-track stripes. (Bottom) SatERR-simulated striping, showing clear striping features and quantitative information.

Fig. 6 shows the striping of MetOp-A MHS 157-GHz observations. Noticeable striping is observed in the Earth-scene brightness temperature. The stripes become more evident with O-B.

Accepted for publication in *Bulletin of the American Meteorological Society*. DOI 10.1175/BAMS-D-22-0207.1.

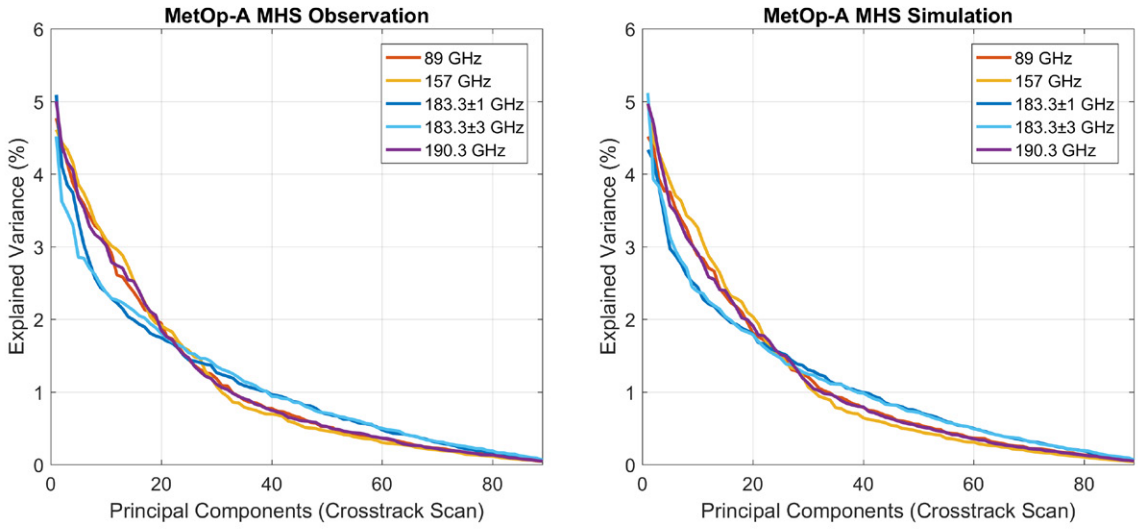

FIG. 7. Principal component decomposition of MetOp-A MHS striping from observations and simulations based on warm load brightness temperatures. The two 183-GHz channels are distinct from the other three channels. Channels 89, 157, and 190 GHz show more pronounced 1/f noise, with the first several principle components (¡ 20) showing more steepness. Simulations agree well with observations.

The simulated striping for the Earth scene is shown at the bottom of Fig. 6. The striping features are resolved with the simulation. Thermal and 1/f noise and orbital oscillation are considered in the simulation with magnitudes extracted from the warm load. The striping magnitude from 1/f noise is 1.6 K, with a total noise of 2.1 K.

Fig. 7 shows the explained variance of PCA-decomposed striping in the warm load from observations (left) and simulations (right). There are two families of channels: The two 183-GHz channels are distinct from the other three channels. Channels 89, 157, and 190.3 GHz have more striping noise, noting that the first few principal components stand out. In the presence of purely white noise, the explained variance would be flat. The simulation is in a consistent agreement with observation.

Channel Crosstalk

We refer to interchannel correlation as a broad phenomenon showing the correlation between channels in terms of brightness temperature, noise, or gain found in hardware and data assimilation, which can arise from a range of sources. We present a specific case relevant to channel

Accepted for publication in *Bulletin of the American Meteorological Society.* DOI 10.1175/BAMS-D-22-0207.1.

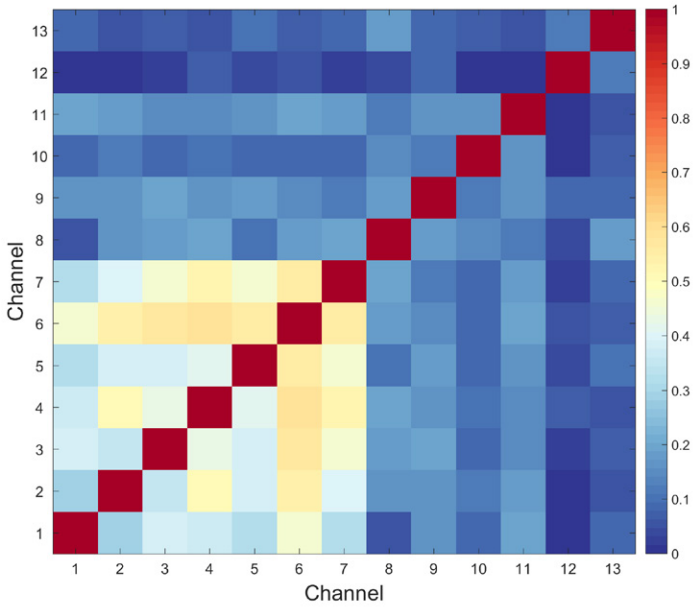

FIG. 8. MWTS-2 channel correlation from sensor warm load measurements.

crosstalk in hardware, noting that there could be different mechanisms for interpreting channel crosstalk. We present a couple of models for simulation channel crosstalk and are cautious that inter-channel correlation can arise from different mechanisms. This error has been found in many radiometers, such as the MicroWave Temperature Sounder II (MWTS-2), the Advanced Technology Micrwave Sounder (ATMS), and the Microwave Humidity Sounder (MHS), where MWTS shows a pronounced correlation in the Earth scene brightness temperature and ATMS and MHS only exhibit noise correlation not affecting scene brightness temperature (Kim et al. 2014; Lu et al. 2015a). Accounting for the interchannel error correlation can improve data assimilation compared to using uncorrelated error covariance. A number of methods have been developed to diagnose interchannel correlation and its error covariance (Hollingsworth and Lönnberg 1986; Desroziers et al. 2005; Stewart et al. 2014; Bormann and Bauer 2010).

We evaluated the impact of channel crosstalk in MWTS-2 on its radiance and science data using SatERR. Fig. 8 presents MWTS-2 interchannel correlations based on in-orbit warm load measurements, showing pronounced correlations between channels 1-7 (Lu et al. 2015a). Measurements exclude the correlation due to spatial correlation or the observation operator error in data assimilation. We fed the measured correlation matrix into SatERR and performed the simulation down to counts which are processed to antenna temperature and brightness temperature through

Accepted for publication in *Bulletin of the American Meteorological Society*. DOI 10.1175/BAMS-D-22-0207.1.

calibration (Corbella et al. 2002; Lu et al. 2015a). The model details are shown in the User Manual (subsection Crosstalk). In our model, we attribute the interchannel correlation to the reflection due to impedance mismatch between the antenna sub-system and receiver front-end, which reflects the carrier frequency of the local oscillator together with signals to the receiver and causes channel crosstalk. In the ground test, the reflection can be measured and represented by S-parameter (Corbella et al. 2002). A small reflection is not appreciable in Earth-scene radiances that have large dynamics, but could still be detected in warm-load/cold-space radiances that are relatively stable.

Fig. 9 illustrates simulated MWTS-2 brightness temperatures on 1 September 2019. Hourly European Centre for Medium-Range Weather Forecasts analysis data with 137 vertical levels and a spatial resolution of 0.25×0.25° are used. The Fast Microwave Emissivity Model 5 is used over the ocean (Liu et al. 2010), and a constant emissivity of 0.9 is used over land. The simulation is performed with the channel crosstalk turned on and off. Fig. 9c illustrates the error at 55.5 GHz (channel 7). There is a noticeable land-ocean contrast, with more negative biases over land, suggesting a surface emission dependency. The 55.5-GHz (channel 7) is supposed to be insensitive to surface emissions because it has a weighting function peaking at 100 mb. However, crosstalk causes channel interference, and channels like 55.5 GHz are affected by surface-sensitive channels. Our simulation is consistent with MWTS-2 observations, where a land-ocean dependency with relatively negative biases over land was found (Lu et al. 2015b). Fig. 10 shows the retrieved atmospheric temperature. A retrieval algorithm developed at NOAA based on empirical regression is used (Zhu and Weng 2013). The error at 50 mb (Fig. 10c) is land-ocean dependent, with the land biased more negative. This is due to the channel crosstalk and the error propagation from radiance to retrieval.

This example suggests that channel crosstalk has a non-trivial impact on radiance and science products. Channels for upper atmosphere sounding can be affected by surface channels, and vice versa, due to channel crosstalk. The error can propagate from radiance to retrieval products, which needs to be included in data assimilation. Since there are many diagnostics for determining channel crosstalk with satellite radiance data, our simulation can be used as ground truth to validate and improve these diagnostics. Our simulation can be used to attribute patterns seen, for instance, in differences between observations and short-range forecasts to certain error sources. A covariance

Accepted for publication in *Bulletin of the American Meteorological Society.* DOI 10.1175/BAMS-D-22-0207.1.

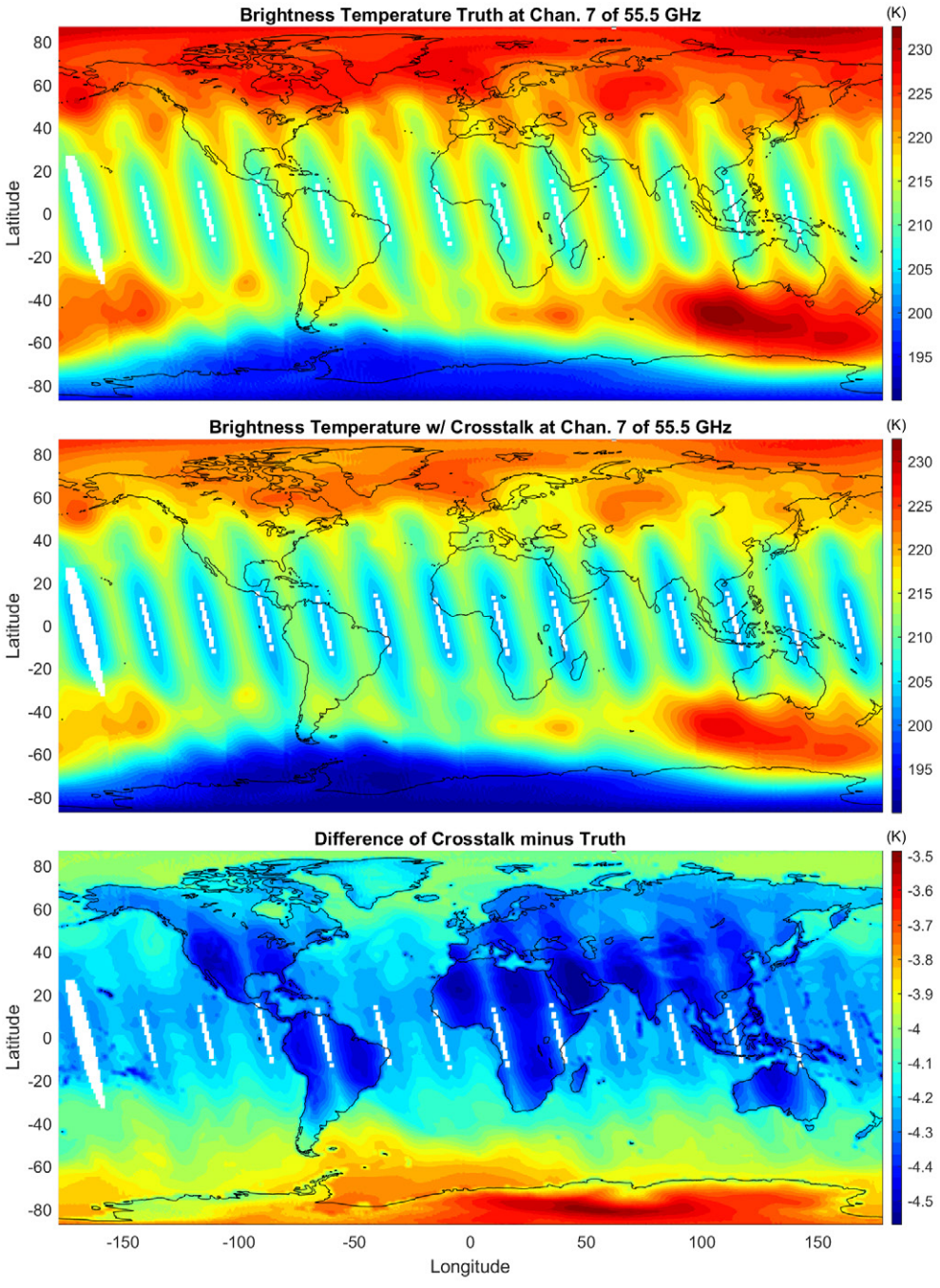

FIG. 9. The impact of channel crosstalk on brightness temperature. (a) Simulated MWTS-2 55.5-GHz (channel 7) brightness temperature free of channel crosstalk. (b) Retrieved brightness temperatures with channel crosstalk. (c) Error-added minus error-free brightness temperatures. A land-ocean contrast is seen due to the impact of low-frequency channels sensitive to surface emissions.

Accepted for publication in *Bulletin of the American Meteorological Society.* DOI 10.1175/BAMS-D-22-0207.1.

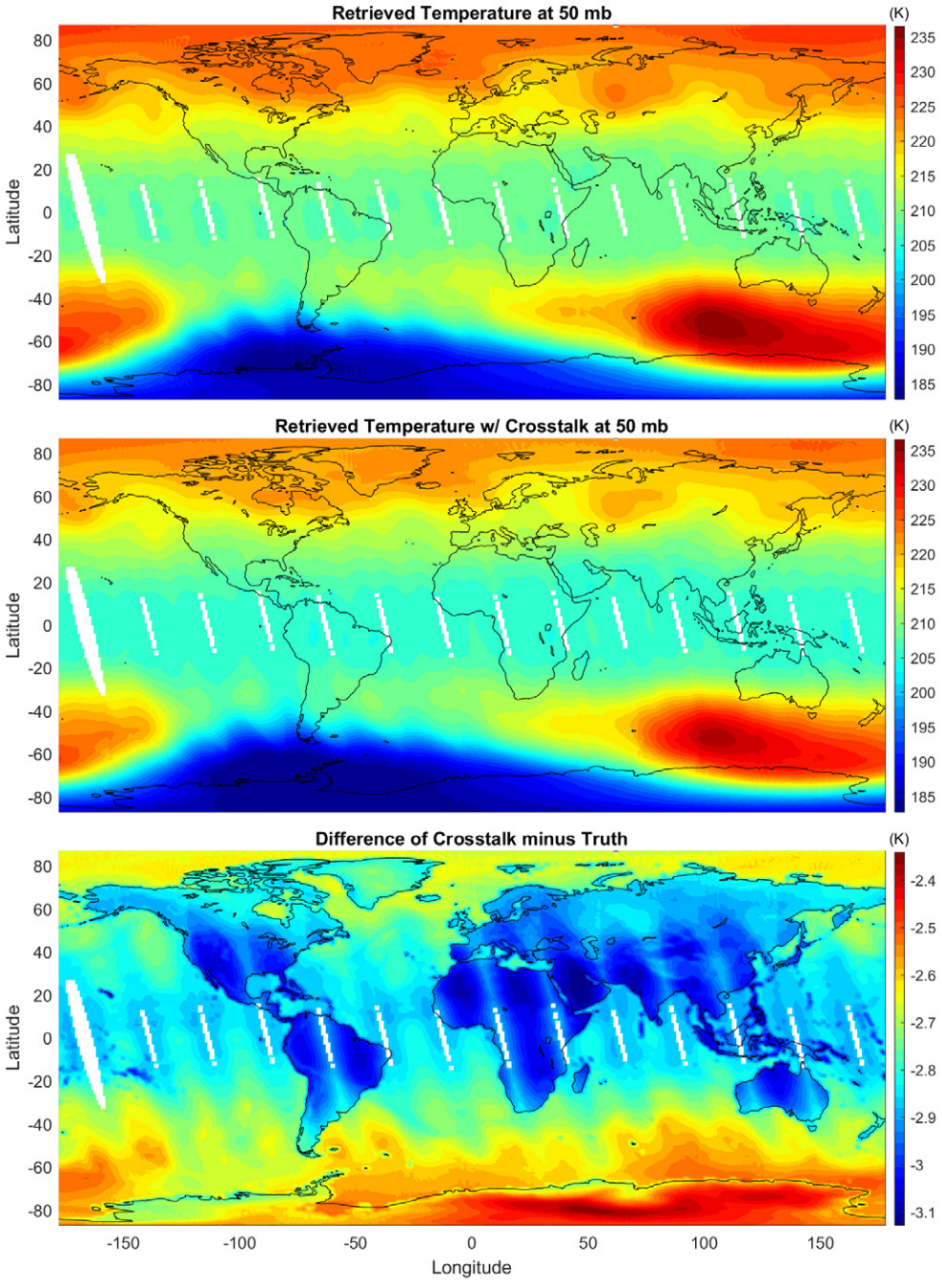

FIG. 10. The impact of channel crosstalk on retrieved atmospheric temperature at 50 mb. (a) Retrieved reference temperatures free of channel crosstalk. (b) Retrieved temperature suffering from channel crosstalk. (c) Error-added minus error-free temperature.

Accepted for publication in *Bulletin of the American Meteorological Society.* DOI 10.1175/BAMS-D-22-0207.1.

matrix for retrieval and data assimilation can be estimated under different error sources. The source attribution also facilitates cal/val activities.

4. Concluding Remarks

The representation and quantification of satellite observation errors are critical for weather forecasting, data assimilation, EDR/CDR products, and hardware development. Observation errors can arise from a range of sources, making them difficult to quantify and partition. Empirical observation error covariances and fixed uncertainties are often used for assimilating satellite data and for quantifying the uncertainties of EDRs/CDRs. However, they cannot accurately represent various error sources because most observation errors are situation dependent. Simulating pixel-level errors and uncertainties with physical models is desirable. A lack of collaborative efforts within the science community poses additional barriers to understanding error propagation at different stages.

We have developed a comprehensive error inventory, SatERR, which can generate a range of observation errors and propagate them to radiance and science products. This is a bottom-up approach, which complements the top-down approach of current diagnostics that inversely solves for errors. SatERR can simulate over 30 errors using mostly physical models. The impact of individual and compound error sources can be quantified in support of data assimilation and EDR/CDR products. Ground-truth testbeds can be produced for validating and refining diagnostics. SatERR can also be used to identify and characterize errors for improving calibration and hardware development. It can be applied to existing sensors or developing new satellite systems. The error inventory is available on GitHub and can be easily expanded. Engineers and scientists working at different stages of satellite data chain can contribute to the error inventory by adding new error sources and models. SatERR contains many microwave sensors onboard traditional and small satellites and can also be used for the development and analysis of new sensors and systems. Apart from bias correction in data assimilation, SatERR can develop situation-dependent error models that capture leading features of the most important errors in a statistical sense separating random and systematic components, and these could then be adopted in the assimilation algorithm. The derived statistical errors can also be used in 1DVar-based retrieval algorithms to improve retrievals. In addition, SatERR can provide users with values of the most important error terms on

Accepted for publication in *Bulletin of the American Meteorological Society.* DOI 10.1175/BAMS-D-22-0207.1.

an observation-by-observation basis. Moving forward, we anticipate to engage more scientists to improve the error inventory and advance satellite-associated observation error quantification.

Accepted for publication in *Bulletin of the American Meteorological Society.* DOI 10.1175/BAMS-D-22-0207.1.

Acknowledgments. This work is supported by NOAA grant NA19NES4320002 through the Cooperative Institute for Satellite Earth System Studies (CICESS) at the University of Maryland/ ESSIC and NASA grant 80NSSC20K0903 from the Weather and Atmospheric Dynamics program.

Data availability statement. SatERR is open source on GitHub (`https://github.com/jxyangrs/saterr`), with technical details in the User Manual `https://github.com/jxyangrs/saterr/blob/main/manual_saterr.pdf`. All the other data and models are freely available online. The ERA5 data and RTTOV are available from ECMWF. CRTM is available from NOAA.

APPENDIX

List of SatERR error sources

Table A1 lists various error sources which are contained in corresponding modules in Figure 3. More details about these errors and models can be referred to User Manual. Regarding horizontal spatial correlation in Table A1, a FOV has a finite size, e.g., the FOV main beam at V-band can be as large as 70 km at off-nadir views. Adjacent FOVs can overlap horizontally, causing correlation. To account for it, we can divide a single FOV into sub-grid, perform simulation at each sub-grid, and sum the simulations weighted by the antenna pattern (Yang and Yang 2018). The vertical overlap of channel weighting functions, as it stands, causes interchannel correlation of Earth-scene radiance, which is different from hardware channel crosstalk.

Accepted for publication in *Bulletin of the American Meteorological Society.* DOI 10.1175/BAMS-D-22-0207.1.

TABLE A1. The SatERR Observation Error Inventory. The error category each error falls into is marked by E1-4, representing measurement, observation operator, representativeness, and preprocessing errors, respectively.

No.	Error and Uncertainty Sources	Description
1	E1: instrument stationary noise	thermal noise, quantization noise in analog-to-digit conversion, etc.
2	E1: instrument non-stationary noise	1/f noise, shot noise, etc.
3	E1: local-oscillator noise	LO noise such as random walk FM, flicker FM, white FM, flicker PM
4	E1: warm load noise	noise in the warm load
5	E1: gain jump	abrupt changes in the power gain
6	E1: receiver nonlinearity	radiometric nonlinearity of the receiver
7	E1: striping	radiometric stripes related to 1/f noise, thermal noise, and calibration
8	E1&2: spectral response	bandpass spectral characteristics that are channel dependent
9	E1&2: scanning and pointing	scanning angle error for viewing cold/warm references, Earth scene
10	E1: orbital oscillation	oscillation of warm load, receiver temperature, gain
11	E1: twist angle offset	offsets in polarization alignment angle, reflector angle, scan angle
12	E1: cross polarization	cross-polarization leakage to neighboring channels
13	E1: cross talk	channel cross talk
14	E1: reflector emission	main reflector emission
15	E1: cold-space mirror emission	cold-space mirror emission
16	E1: warm load errors	non-ideal blackbody emissivity, bias (e.g. solar intrusion)
17	E1: spillover	spillover seeing cosmic background
18	E1: FOV intrusion	field of view intrusion due to the spacecraft or payloads
19	E1: payload interference	interference from onboard instruments
20	E1&2: spacecraft attitude offset	roll, pitch, yaw
21	E1&2: Faraday rotation	Faraday rotation due to ionosphere and Earth's magnetic field
22	E1: count to antenna temperature	calibration frequency, windowing function, etc.
23	E1: antenna pattern correction	calibrating antenna temperature to brightness temperature
24	E1: gain and noise long-term change	long-term degradation in terms of noise and gain
25	E1&2: frequency drift	channel center frequency drift
26	E1&2: orbit drift	long-term satellite altitude change
27	E2: horizontal spatial correlation	FOV overlap horizontally that can be simulated w/ antenna pattern
28	E2: vertical spatial correlation	vertical overlap of channel weighting functions
29	E2: surface and atmospheric profile uncertainties	errors in surface and atmospheric profiles
30	E2&3: RTM error	RTM deficiencies in surface, atmospheric, and cloud models
31	E2&3: spatial resolution in RTM	vertical or horizontal resolutions affecting RTM simulations
32	E2: collocation	collocation criteria for single or multiple satellites
33	E2: intercalibration	errors due to sensor difference in frequency, scanning angle, collocation criteria, RTM
34	E4: prescreening	filtering and screening for satellite data
35	E3&4: retrieval	inversion based retrieval affecting EDR and CDR
36	E2-4: external models, algorithms	combining our simulator with external RTM, retrieval algorithms

References

Ablain, M., and Coauthors, 2015: Improved sea level record over the satellite altimetry era (1993–2010) from the climate change initiative project. *Ocean Science*, **11 (1)**, 67–82.

Accepted for publication in *Bulletin of the American Meteorological Society.* DOI 10.1175/BAMS-D-22-0207.1.

Alquaied, F., R. Chen, and W. L. Jones, 2018: Hot load temperature correction for trmm microwave imager in the legacy brightness temperature. *IEEE Journal of Selected Topics in Applied Earth Observations and Remote Sensing*, **11 (6)**, 1923–1931.

Balanis, C. A., 2015: *Antenna theory: analysis and design*. John wiley & sons.

Bell, W., and Coauthors, 2008: The assimilation of ssmis radiances in numerical weather prediction models. *IEEE Transactions on Geoscience and Remote Sensing*, **46 (4)**, 884–900.

Bellprat, O., F. Massonnet, S. Siegert, C. Prodhomme, D. Macias-Gómez, V. Guemas, and F. Doblas-Reyes, 2017: Uncertainty propagation in observational references to climate model scales. *Remote Sensing of Environment*, **203**, 101–108.

Berg, W., and Coauthors, 2016: Intercalibration of the gpm microwave radiometer constellation. *Journal of Atmospheric and Oceanic Technology*, **33 (12)**, 2639–2654.

Bormann, 2020: A review of the evolution of setting observation errors in satellite DA. *ECMWF/EUMETSAT NWP SAF Workshop on the treatment of random and systematic errors in satellite data assimilation for NWP*.

Bormann, N., and P. Bauer, 2010: Estimates of spatial and interchannel observation-error characteristics for current sounder radiances for numerical weather prediction. i: Methods and application to atovs data. *Quarterly Journal of the Royal Meteorological Society*, **136 (649)**, 1036–1050.

Bormann, N., A. Fouilloux, and W. Bell, 2013: Evaluation and assimilation of atms data in the ecmwf system. *Journal of Geophysical Research: Atmospheres*, **118 (23)**, 12–970.

Boukabara, S.-A., and Coauthors, 2011: Mirs: An all-weather 1dvar satellite data assimilation and retrieval system. *IEEE Transactions on Geoscience and Remote Sensing*, **49 (9)**, 3249–3272.

Cai, G., B. M. Chen, and T. H. Lee, 2011: *Unmanned rotorcraft systems*. Springer Science & Business Media.

Campbell, W. F., E. A. Satterfield, B. Ruston, and N. L. Baker, 2017: Accounting for correlated observation error in a dual-formulation 4d variational data assimilation system. *Monthly Weather Review*, **145 (3)**, 1019–1032.

Accepted for publication in *Bulletin of the American Meteorological Society*. DOI 10.1175/BAMS-D-22-0207.1.

Carrassi, A., M. Bocquet, L. Bertino, and G. Evensen, 2018: Data assimilation in the geosciences: An overview of methods, issues, and perspectives. *Wiley Interdisciplinary Reviews: Climate Change*, **9 (5)**, e535.

Chander, G., T. J. Hewison, N. Fox, X. Wu, X. Xiong, and W. J. Blackwell, 2013: Overview of intercalibration of satellite instruments. *IEEE Transactions on Geoscience and Remote Sensing*, **51 (3)**, 1056–1080.

Christy, J. R., R. W. Spencer, and W. D. Braswell, 1997: How accurate are satellite 'thermometers'? *Nature*, **389 (6649)**, 342–342.

Chun, H.-W., R. Eresmaa, A. P. McNally, N. Bormann, and M. Matricardi, 2015: A physically-based observation-error covariance matrix for iasi. *The 20th International TOVS Study Conference (ITSC-20)*, Vol. 27.

Colton, M. C., and G. A. Poe, 1999: Intersensor calibration of dmsp ssm/i's: F-8 to f-14, 1987-1997. *IEEE Transactions on Geoscience and Remote Sensing*, **37 (1)**, 418–439.

Corbella, I., A. J. Gasiewski, M. Klein, V. Leuski, A. J. Francavilla, and J. R. Piepmeier, 2002: On-board accurate calibration of dual-channel radiometers using internal and external references. *IEEE transactions on microwave theory and techniques*, **50 (7)**, 1816–1820.

Davis, W. A., and K. K. Agarwal, 2011: *Radio Frequency Circuit Design*. 2nd ed., Wiley, New York, https://doi.org/10.1002/0471200689.

Dee, D., M. Balmaseda, G. Balsamo, R. Engelen, A. Simmons, and J.-N. Thépaut, 2014: Toward a consistent reanalysis of the climate system. *Bulletin of the American Meteorological Society*, **95 (8)**, 1235–1248.

Desroziers, G., L. Berre, B. Chapnik, and P. Poli, 2005: Diagnosis of observation, background and analysis-error statistics in observation space. *Quarterly Journal of the Royal Meteorological Society: A journal of the atmospheric sciences, applied meteorology and physical oceanography*, **131 (613)**, 3385–3396.

Draper, D. W., D. A. Newell, F. J. Wentz, S. Krimchansky, and G. M. Skofronick-Jackson, 2015: The global precipitation measurement (gpm) microwave imager (gmi): Instrument overview and

Accepted for publication in *Bulletin of the American Meteorological Society.* DOI 10.1175/BAMS-D-22-0207.1.

early on-orbit performance. *IEEE Journal of Selected Topics in Applied Earth Observations and Remote Sensing*, **8 (7)**, 3452–3462.

Elsaesser, G. S., 2006: A parametric optimal estimation retrieval of the non-precipitating parameters over the global oceans. Masters Thesis, Colorado State University.

Gaiser, P. W., and Coauthors, 2004: The windsat spaceborne polarimetric microwave radiometer: Sensor description and early orbit performance. *IEEE Transactions on Geoscience and Remote Sensing*, **42 (11)**, 2347–2361.

Geer, A. J., and P. Bauer, 2011: Observation errors in all-sky data assimilation. *Quarterly Journal of the Royal Meteorological Society*, **137 (661)**, 2024–2037.

Geer, A. J., P. Bauer, and N. Bormann, 2010: Solar biases in microwave imager observations assimilated at ecmwf. *IEEE transactions on geoscience and remote sensing*, **48 (6)**, 2660–2669.

Geer, A. J., and Coauthors, 2018: All-sky satellite data assimilation at operational weather forecasting centres. *Quarterly Journal of the Royal Meteorological Society*, **144 (713)**, 1191–1217.

Goodberlet, M., C. Swift, and J. Wilkerson, 1989: Remote sensing of ocean surface winds with the special sensor microwave/imager. *Journal of Geophysical Research: Oceans*, **94 (C10)**, 14 547–14 555.

Gopalan, K., W. L. Jones, S. Biswas, S. Bilanow, T. Wilheit, and T. Kasparis, 2009: A time-varying radiometric bias correction for the trmm microwave imager. *IEEE transactions on geoscience and remote sensing*, **47 (11)**, 3722–3730.

Griffin, M. D., 2004: *Space vehicle design*. AIAA.

Gruber, A., and Coauthors, 2020: Validation practices for satellite soil moisture retrievals: What are (the) errors? *Remote sensing of environment*, **244**, 111 806.

Han, Y., 2006: Jcsda community radiative transfer model (crtm): Version 1.

Hollingsworth, A., and P. Lönnberg, 1986: The statistical structure of short-range forecast errors as determined from radiosonde data. part i: The wind field. *Tellus A*, **38 (2)**, 111–136.

Hollmann, R., and Coauthors, 2013: The esa climate change initiative: Satellite data records for essential climate variables. *Bulletin of the American Meteorological Society*, **94 (10)**, 1541–1552.

Accepted for publication in *Bulletin of the American Meteorological Society*. DOI 10.1175/BAMS-D-22-0207.1.

Hurrell, J. W., and K. E. Trenberth, 1997: Spurious trends in satellite msu temperatures from merging different satellite records. *Nature*, **386 (6621)**, 164–167.

Janjić, T., and Coauthors, 2018: On the representation error in data assimilation. *Quarterly Journal of the Royal Meteorological Society*, **144 (713)**, 1257–1278.

Janssen, M. A., C. S. Ruf, and S. J. Keihm, 1995: Topex/poseidon microwave radiometer (tmr). ii. antenna pattern correction and brightness temperature algorithm. *IEEE transactions on geoscience and remote sensing*, **33 (1)**, 138–146.

Jarnot, R., R. Cofield, J. Waters, D. Flower, and G. E. Peckham, 1996: Calibration of the microwave limb sounder on the upper atmosphere research satellite. *Journal of Geophysical Research: Atmospheres*, **101 (D6)**, 9957–9982.

Joo, S., J. Eyre, and R. Marriott, 2013: The impact of metop and other satellite data within the met office global nwp system using an adjoint-based sensitivity method. *Monthly weather review*, **141 (10)**, 3331–3342.

Kalnay, E., 2003: *Atmospheric modeling, data assimilation and predictability*. Cambridge university press.

Kalnay, E., and Coauthors, 1996: The ncep/ncar 40-year reanalysis project. *Bulletin of the American meteorological Society*, **77 (3)**, 437–472.

Kim, E., C.-H. J. Lyu, K. Anderson, R. Vincent Leslie, and W. J. Blackwell, 2014: S-npp atms instrument prelaunch and on-orbit performance evaluation. *Journal of Geophysical Research: Atmospheres*, **119 (9)**, 5653–5670.

Kroodsma, R. A., D. S. McKague, and C. S. Ruf, 2012: Inter-calibration of microwave radiometers using the vicarious cold calibration double difference method. *IEEE Journal of Selected Topics in Applied Earth Observations and Remote Sensing*, **5 (3)**, 1006–1013.

Langland, R. H., and N. L. Baker, 2004: Estimation of observation impact using the nrl atmospheric variational data assimilation adjoint system. *Tellus A: Dynamic Meteorology and Oceanography*, **56 (3)**, 189–201.

Accepted for publication in *Bulletin of the American Meteorological Society.* DOI 10.1175/BAMS-D-22-0207.1.

Lee, T. H., 2004: *The Design of CMOS Radio-Frequency Integrated Circuits*. Cambridge Univ, https://doi.org/10.1017/cbo9780511817281.

Lee, Y.-K., C. Grassotti, Q. Liu, S.-Y. Liu, and Y. Zhou, 2022: In-depth evaluation of mirs total precipitable water from noaa-20 atms using multiple reference data sets. *Earth and Space Science*, **9 (2)**, e2021EA002 042.

Liu, E., C. Andrew, S. Scott, and L. Haixia, 2022: A revised all-sky radiance assimilation framework in the ncep global forecast system. *Global Space-based Inter-Calibration System - Microwave Subgroup Workshop Past, Current, and Future Applications of Microwave Data*.

Liu, Q., F. Weng, and S. J. English, 2010: An improved fast microwave water emissivity model. *IEEE Transactions on Geoscience and Remote Sensing*, **49 (4)**, 1238–1250.

Liu, S., C. Grassotti, Q. Liu, Y.-K. Lee, R. Honeyager, Y. Zhou, and M. Fang, 2020: The noaa microwave integrated retrieval system (mirs): Validation of precipitation from multiple polar-orbiting satellites. *IEEE Journal of Selected Topics in Applied Earth Observations and Remote Sensing*, **13**, 3019–3031.

Lu, L., Q., B. H., S. N., English, K. Lean, N. Atkinson, W. Bell, and F. Carminati, 2015a: An evaluation of fy-3c satellite data quality at ecmwf and the met office.

Lu, Q., and W. Bell, 2014: Characterizing channel center frequencies in amsu-a and msu microwave sounding instruments. *Journal of Atmospheric and Oceanic Technology*, **31 (8)**, 1713–1732.

Lu, Q., H. Lawrence, N. Bormann, S. English, K. Lean, N. Atkinson, W. Bell, and F. Carminati, 2015b: *An evaluation of FY-3C satellite data quality at ECMWF and the Met Office*, Vol. 767. European Centre for Medium-Range Weather Forecasts Reading, UK.

Ma, Y., and X. Zou, 2015: Striping noise mitigation in atms brightness temperatures and its impact on cloud lwp retrievals. *Journal of Geophysical Research: Atmospheres*, **120 (13)**, 6634–6653.

McKague, D. S., C. S. Ruf, and J. J. Puckett, 2010: Beam spoiling correction for spaceborne microwave radiometers using the two-point vicarious calibration method. *IEEE transactions on geoscience and remote sensing*, **49 (1)**, 21–27.

Accepted for publication in *Bulletin of the American Meteorological Society.* DOI 10.1175/BAMS-D-22-0207.1.

Mears, C. A., and F. J. Wentz, 2017: A satellite-derived lower-tropospheric atmospheric temperature dataset using an optimized adjustment for diurnal effects. *Journal of Climate*, **30 (19)**, 7695–7718.

Meissner, T., and F. J. Wentz, 2006: Polarization rotation and the third stokes parameter: The effects of spacecraft attitude and faraday rotation. *IEEE Transactions on Geoscience and Remote Sensing*, **44 (3)**, 506–515.

Merchant, C. J., and Coauthors, 2017: Uncertainty information in climate data records from earth observation. *Earth System Science Data*, **9 (2)**, 511–527.

Merchant, C. J., and Coauthors, 2019: Satellite-based time-series of sea-surface temperature since 1981 for climate applications. *Scientific data*, **6 (1)**, 1–18.

Mittaz, J., C. J. Merchant, and E. R. Woolliams, 2019: Applying principles of metrology to historical earth observations from satellites. *Metrologia*, **56 (3)**, 032 002.

Mo, T., 1996: Prelaunch calibration of the advanced microwave sounding unit-A for NOAA-K. *IEEE Transactions on Microwave theory and Techniques*, **44 (8)**, 1460–1469.

National Research Council, 2007: *Completing the forecast: Characterizing and communicating uncertainty for better decisions using weather and climate forecasts*. National Academies Press, 76 pp.

Newman, M., P. D. Sardeshmukh, and J. W. Bergman, 2000: An assessment of the ncep, nasa, and ecmwf reanalyses over the tropical west pacific warm pool. *Bulletin of the American Meteorological Society*, **81 (1)**, 41–48.

Njoku, E. G., 1980: Antenna pattern correction procedures for the scanning multichannel microwave radiometer (smmr). *Boundary-Layer Meteorology*, **18 (1)**, 79–98.

Njoku, E. G., P. Ashcroft, T. K. Chan, and L. Li, 2005: Global survey and statistics of radio-frequency interference in amsr-e land observations. *IEEE Transactions on Geoscience and Remote Sensing*, **43 (5)**, 938–947.

Accepted for publication in *Bulletin of the American Meteorological Society.* DOI 10.1175/BAMS-D-22-0207.1.

Piepmeier, J. R., and Coauthors, 2013: Radio-frequency interference mitigation for the soil moisture active passive microwave radiometer. *IEEE Transactions on Geoscience and Remote Sensing*, **52 (1)**, 761–775.

Piepmeier, J. R., and Coauthors, 2017: Smap l-band microwave radiometer: Instrument design and first year on orbit. *IEEE Transactions on Geoscience and Remote Sensing*, **55 (4)**, 1954–1966.

Popp, T., and Coauthors, 2020: Consistency of satellite climate data records for earth system monitoring. *Bulletin of the American Meteorological Society*, **101 (11)**, E1948–E1971.

Qin, Z., X. Zou, and F. Weng, 2013: Analysis of atms striping noise from its earth scene observations. *Journal of Geophysical Research: Atmospheres*, **118 (23)**, 13–214.

Rosenkranz, P., 2017: Line-by-line microwave radiative transfer (non-scattering). *Remote Sensing Code Library, https://doi. org/10.21982 M*, **81013**.

Rosenkranz, P. W., 2006: Cloud liquid-water profile retrieval algorithm and validation. *Journal of Geophysical Research: Atmospheres*, **111 (D9)**.

Rosenkranz, P. W., and D. Cimini, 2019: Speed dependence of 22-and 118-ghz line shapes for tropospheric remote sensing. *IEEE Transactions on Geoscience and Remote Sensing*, **57 (12)**, 9702–9708.

Ruf, C. S., S. J. Keihm, and M. A. Janssen, 1995: Topex/poseidon microwave radiometer (tmr). i. instrument description and antenna temperature calibration. *IEEE Transactions on Geoscience and Remote sensing*, **33 (1)**, 125–137.

Saha, S., and Coauthors, 2010: The ncep climate forecast system reanalysis. *Bulletin of the American Meteorological Society*, **91 (8)**, 1015–1058.

Santer, B. D., and Coauthors, 2017: Causes of differences in model and satellite tropospheric warming rates. *Nature Geoscience*, **10 (7)**, 478–485.

Saunders, R., and Coauthors, 2018: An update on the rttov fast radiative transfer model (currently at version 12). *Geoscientific Model Development*, **11 (7)**, 2717–2737.

Spencer, R. W., and J. R. Christy, 1992a: Precision and radiosonde validation of satellite gridpoint temperature anomalies. part i: Msu channel 2. *Journal of Climate*, **5 (8)**, 847–857.

Accepted for publication in *Bulletin of the American Meteorological Society*. DOI 10.1175/BAMS-D-22-0207.1.

Spencer, R. W., and J. R. Christy, 1992b: Precision and radiosonde validation of satellite gridpoint temperature anomalies. part ii: A tropospheric retrieval and trends during 1979–90. *Journal of Climate*, **5 (8)**, 858–866.

Stewart, L., S. L. Dance, N. K. Nichols, J. Eyre, and J. Cameron, 2014: Estimating interchannel observation-error correlations for iasi radiance data in the met office system. *Quarterly Journal of the Royal Meteorological Society*, **140 (681)**, 1236–1244.

Thébault, E., and Coauthors, 2015: International geomagnetic reference field: the 12th generation. *Earth, Planets and Space*, **67 (1)**, 1–19.

Twarog, E. M., W. E. Purdy, P. W. Gaiser, K. H. Cheung, and B. E. Kelm, 2006: Windsat on-orbit warm load calibration. *IEEE Transactions on Geoscience and Remote Sensing*, **44 (3)**, 516–529.

Vinnikov, K. Y., and N. C. Grody, 2003: Global warming trend of mean tropospheric temperature observed by satellites. *Science*, **302 (5643)**, 269–272.

Weng, F., 2015: Atms sdr overview. STAR JPSS 2015 Annual Science Team Meeting.

Weng, F., L. Zhao, R. R. Ferraro, G. Poe, X. Li, and N. C. Grody, 2003: Advanced microwave sounding unit cloud and precipitation algorithms. *Radio Science*, **38 (4)**.

Weng, F., and Coauthors, 2013: Calibration of suomi national polar-orbiting partnership advanced technology microwave sounder. *Journal of Geophysical Research: Atmospheres*, **118 (19)**, 11–187.

Wentz, F. J., P. Ashcroft, and C. Gentemann, 2001: Post-launch calibration of the trmm microwave imager. *IEEE Transactions on Geoscience and Remote Sensing*, **39 (2)**, 415–422.

Wentz, F. J., and D. Draper, 2016: On-orbit absolute calibration of the global precipitation measurement microwave imager. *Journal of Atmospheric and Oceanic Technology*, **33 (7)**, 1393–1412.

Wentz, F. J., and M. Schabel, 1998: Effects of orbital decay on satellite-derived lower-tropospheric temperature trends. *Nature*, **394 (6694)**, 661–664.

Accepted for publication in *Bulletin of the American Meteorological Society.* DOI 10.1175/BAMS-D-22-0207.1.

Yan, B., and K. Ahmad, 2020: Derivation and validation of sensor brightness temperatures for advanced microwave sounding unit-a instruments. *IEEE Transactions on Geoscience and Remote Sensing*, **59 (1)**, 404–414.

Yang, J. X., and D. S. McKague, 2016: Improving collocation-based scan-dependent intercalibration over the ocean for spaceborne radiometry. *IEEE Geoscience and Remote Sensing Letters*, **13 (4)**, 589–593.

Yang, J. X., D. S. Mckague, and C. S. Ruf, 2014: Land contamination correction for passive microwave radiometer data: Demonstration of wind retrieval in the great lakes using ssm/i. *Journal of Atmospheric and Oceanic Technology*, **31 (10)**, 2094–2113.

Yang, J. X., D. S. McKague, and C. S. Ruf, 2015a: Boreal, temperate, and tropical forests as vicarious calibration sites for spaceborne microwave radiometry. *IEEE Transactions on Geoscience and Remote Sensing*, **54 (2)**, 1035–1051.

Yang, J. X., D. S. McKague, and C. S. Ruf, 2015b: Identifying and resolving a calibration issue with gmi. *2015 IEEE International Geoscience and Remote Sensing Symposium (IGARSS)*, IEEE, 2568–2571.

Yang, J. X., and H. Yang, 2018: Radiometry calibration with high-resolution profiles of gpm: Application to atms 183-ghz water vapor channels and comparison against reanalysis profiles. *IEEE Transactions on Geoscience and Remote Sensing*, **57 (2)**, 829–838.

Yang, J. X., Y. You, W. Blackwell, S. Misra, and R. A. Kroodsma, 2021: Quantifying and characterizing striping of microwave humidity sounder with observation and simulation. *IEEE Transactions on Geoscience and Remote Sensing*.

Yang, J. X., and Coauthors, 2022: An adaptive calibration window for noise reduction of satellite microwave radiometers. *IEEE Transactions on Geoscience and Remote Sensing*.

Yang, W., H. Meng, R. R. Ferraro, I. Moradi, and C. Devaraj, 2012: Cross-scan asymmetry of amsu-a window channels: Characterization, correction, and verification. *IEEE transactions on geoscience and remote sensing*, **51 (3)**, 1514–1530.

Zhu, T., and F. Weng, 2013: Hurricane sandy warm-core structure observed from advanced technology microwave sounder. *Geophysical Research Letters*, **40 (12)**, 3325–3330.

Accepted for publication in *Bulletin of the American Meteorological Society.* DOI 10.1175/BAMS-D-22-0207.1.

Zou, C.-Z., M. D. Goldberg, and X. Hao, 2018: New generation of us satellite microwave sounder achieves high radiometric stability performance for reliable climate change detection. *Science advances*, **4 (10)**, eaau0049.

Zou, C.-Z., and H. Qian, 2016: Stratospheric temperature climate data record from merged ssu and amsu-a observations. *Journal of Atmospheric and Oceanic Technology*, **33 (9)**, 1967–1984.

Zou, C.-Z., and W. Wang, 2011: Intersatellite calibration of amsu-a observations for weather and climate applications. *Journal of Geophysical Research: Atmospheres*, **116 (D23)**.

Zou, C.-Z., H. Xu, X. Hao, and Q. Fu, 2021: Post-millennium atmospheric temperature trends observed from satellites in stable orbits. *Geophysical Research Letters*, **48 (13)**, e2021GL093 291.

Accepted for publication in *Bulletin of the American Meteorological Society.* DOI 10.1175/BAMS-D-22-0207.1.